IOP Publishing Journal of Optics
J. Opt. 19 (2017) 034002 (5pp) https://doi.org/10.1088/2040-8986/aa587b

Temporal ghost imaging with twin photons

Séverine Denis[1], Paul-Antoine Moreau[2], Fabrice Devaux[1] and Eric Lantz[1]

[1] Institut FEMTO-ST, Département d'Optique P. M. Duffieux, UMR 6174 CNRS Université Bourgogne Franche-Comté, 15b Avenue des Montboucons, F-25030 Besançon, France
[2] SUPA, School of Physics and Astronomy, University of Glasgow, Glasgow G12 8QQ, United Kingdom

E-mail: severine.denis@femto-st.fr

Received 17 December 2016
Accepted for publication 10 January 2017
Published 9 February 2017

Abstract
We use twin photons generated by spontaneous parametric down conversion to perform temporal ghost imaging of a single time signal. The retrieval of a binary signal containing eight bits is performed with an error rate below 1%.

Keywords: quantum ghost imaging, quantum optics, photon statistics, nonlinear optics, parametric processes

(Some figures may appear in colour only in the online journal)

1. Introduction

For the two last decades, ghost imaging has emerged as a kind of magical way to form images of a spatial object, typically a spatially varying transparency, with a single point detector (SPD) that does not have spatial resolution. The initial works used the quantum nature of entanglement of a two-photon state, where photons of a pair are spatially and temporally correlated, to detect temporal coincidences. While one of the photons passing through the object was detected by a photon counter with no spatial resolution, its twin photon was detected with spatial resolution by scanning the transverse plane with a single detector [1], or recently by an intensified charge-coupled device (ICCD) [2]. Later, ghost imaging exploiting the temporal correlations of the intensity fluctuations of classical [3] or pseudothermal light [4] was proposed. The ability to retrieve the object with unity contrast seems to be the only property that belongs to quantum experiments on their own [5].

The extension of ghost imaging to a time object, i.e., a temporally varying transparency, has been recently demonstrated experimentally [6–8]. In [6], the light was transmitted through a 'time object' and detected with a slow SPD which cannot resolve the time object, while in the reference arm, the light that did not interact with the temporal object was detected with a fast SPD. Measurements over several thousand copies of the temporal signal were necessary to retrieve a binary signal with a good signal-to-noise ratio. To retrieve a non-reproducible time object using a single-shot acquisition, we proposed in [7] the exact space–time transposition of computational ghost imaging [9, 10]: a single-shot acquisition of the time object was performed by multiplying it with computer-generated random images, ensuring spatial multiplexing of temporal intensity correlations before detecting the sum image with no temporal resolution. While very simple and costless, this method is slow. To increase the speed to a *kHz* rate, we reported the use of speckle patterns [8], i.e., the temporal transposition of spatial ghost imaging with pseudothermal light [4].

In the present paper, we demonstrate temporal ghost imaging with twin photons generated by spontaneous parametric down conversion (SPDC), i.e., the temporal transposition of the first ghost imaging experiments [1]: while the photons passing through the temporal object are detected by a photon-counting camera with no temporal resolution, their twins do not interact with the object but are detected with temporal and spatial resolution by a second camera. Note that the use of biphotons for temporal imaging has been studied theoretically in [11].

2. Experimental overview

In the setup represented in figure 1, a type-2-oriented beta barium borate (BBO) nonlinear crystal with a diameter of 5 mm and thickness of 0.8 mm is enlightened over its entire surface with a 354.65 nm UV pulsed laser. From their interaction with the BBO, pump photons are annihilated and generate twin photons that form the signal and idler SPDC beams around the degeneracy wavelength of 709.3 nm. The

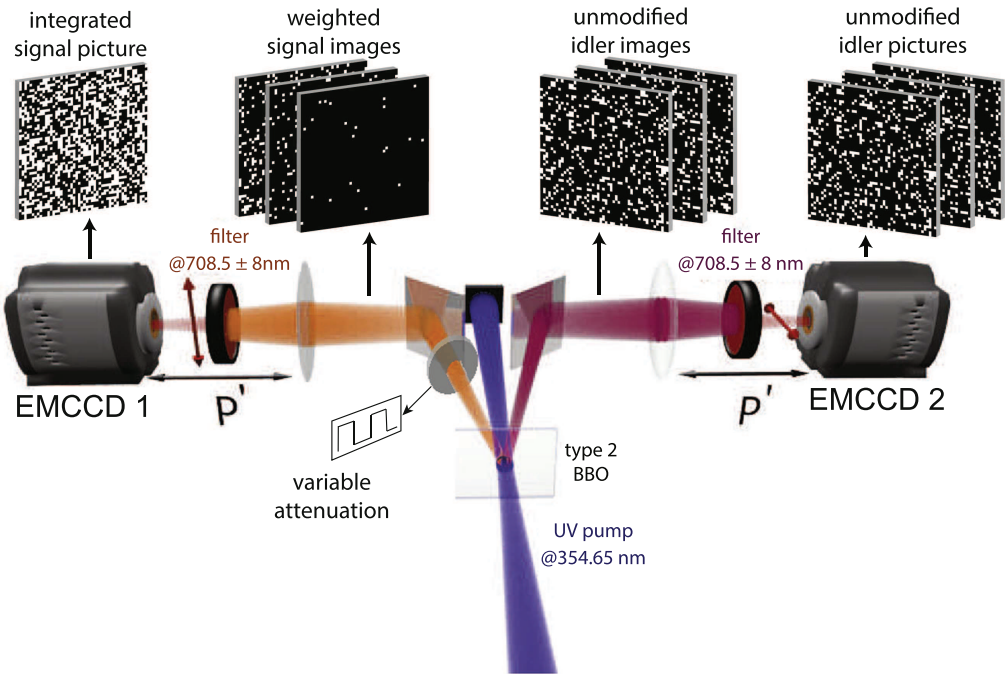

Figure 1. Experimental setup used to record the ghost signal and reference idler images. The red arrows represent the polarization directions of the signal and idler beams. The variable attenuation, made with a liquid crystal variable retarder and a polarizer, is adjusted accordingly.

filters used have a quasi-rectangular spectrum transmission profile centered at 708.5 ± 8 nm, i.e., not exactly at the degeneracy wavelength of the SPDC.

A variable density made with a liquid crystal variable retarder controlled by a function generator, and followed by a polarizer, is placed in the way of the signal beam. Hence, the signal images are first weighted one by one by the variable density whose values are given by the temporal signal to be retrieved, then summed together without any temporal resolution, on an electron multiplying charge-coupled device (EMCCD1). At exactly the same time, the unweighed idler images are acquired one by one by a second camera (EMCCD2) as reference patterns with, for each image I_n, a time exposure synchronized with the step n of the time signal. The signal and idler images are recorded in the image plane of the BBO crystal in order to ensure a good match between the positions of the signal and idler photons in twin images, even if their wavelengths are slightly different due to the 16 nm width filters. The 512×512 pixel EMCCD (Andor iXon3 897) sensors are cooled at $-100\,^{\circ}\mathrm{C}$ and ensure a quantum efficiency over 90% at 708 nm. The photon localizations are recorded by applying a thresholding procedure (as shown in figure 1). The mean flux is set between 0.10 and 0.20 photons per pixel (ph/px) on the sum image, i.e., less on the reference images, in order to minimize the whole number of false detections [12].

The equivalent quantum efficiency η of the setup is given for twin images by the number of detected signal (or idler) photons corresponding to a true pair divided by the total number of detected photons. This parameter takes into account the overall quantum efficiency of the setup, affected by the random absorption of photons by the optical components or no detection by the cameras, but also parasitic fluorescence of the optical components and false decisions during the thresholding procedure. We have shown in [13] that sources of single photons, such as parasitic fluorescence or photons transmitted at the edge of the filters with no transmission at the twin wavelength, have an effect similar to a decrease of the quantum efficiency. Here, the equivalent quantum efficiency of the filters is estimated at 92% and the combined maximum transmission of the retarder and polarizer is estimated at $\eta_L = 81\%$. Noises from the detector, like readout noise or clock-induced charges (CIC), result also in single photoelectrons: either a nongenuine photon is detected (due, for example, to CIC; false positive error) or a genuine photon is not detected because the associated level at the output of the multiplication register remains below the threshold (false negative error). This latter case is directly equivalent to a decrease of the quantum efficiency. The former false positive error cannot be considered equivalent as a variation of the quantum efficiency since its occurrence does not depend on the light flux [13]. However, it does result in the creation of single detected photons and its effect is completely similar to a decrease of the quantum efficiency in integral measurements like those performed in this experiment. The background noises were estimated by recording images with the pump beam off. They are estimated at 0.018 ph/px for the signal image and 0.0064 ph/px for one of the idler images.

The experimental value of η is directly given by the normalized cross-correlation coefficient of the signal and idler pictures. However, in our case, the size of the spatial coherence cells of the SPDC beams does not correspond to the pixels and scales as the inverse of the phase-matching angular range [14]. The cross-correlation then displays a peak with a Gaussian-like shape that spreads on several pixels. To obtain

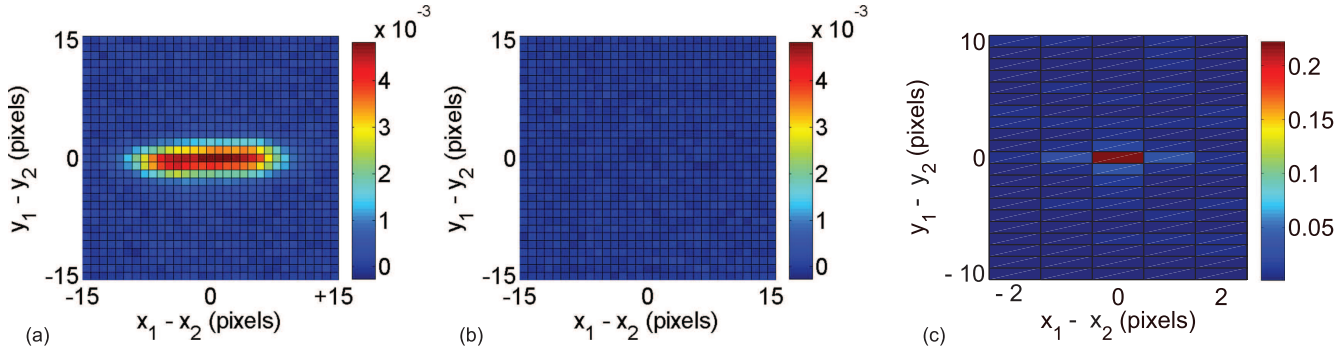

Figure 2. (*a*) Mean on 900 realizations of the normalized cross-correlation coefficient of two twin images, without binning. (*b*) The same for two independent signal and idler images. (*c*) Cross-correlation coefficient of figure (*a*) after a binning of 16 × 5 pixels.

the full cross-correlation peak on one pixel, a grouping (binning) of B pixels of the cross-correlation figure must be performed. To estimate η, we recorded one series of 900 twin images, with no time modulation (transmission set to 1) and the same integration time on each side. The mean filling ratio m_s was set at 0.04 ph/px by adjusting the acquisition time of the cameras. The number of pixels $D = 506 \times 506$ in each picture used for the cross-correlation is then given by the effective area of the camera sensors. The average normalized cross-correlation is given in figure 2. The size of the spatial coherence cell is estimated at $B = 16 \times 5$ pixels. However, the binning of the cross-correlation figure is not used here since the average on 900 cross-correlations allows the distinction of the pixels of the peak from those of the cross-correlation background. The integration of the cross-correlation peak gives an overall equivalent quantum efficiency η of 30.2%.

3. Retrieval of a ghost time signal

After acquisition of the weighted and reference images, the reconstruction of the time signal is performed by computing the cross-correlation of the signal image and each reference idler image. Here, since we use only one pair of images to determine each cross-correlation coefficient, the cross-correlation peak must be binned in order to be distinguished from the cross-correlation background. The successive cross-correlation coefficients are then plotted over the time to retrieve the shape of the time signal.

In an ideal experiment with unity quantum efficiency, a photoelectron detected in the integrated signal image corresponds always to a photon at the same position in one of the reference idler images. However, the random distribution of SPDC photons provides statistically independent photon repartitions for different time steps of the signal and idler or different temporal modes in a single time step. Consequently, two signal and idler photons that are not twins can be situated in a coherence cell at the same position. These photons create accidental matches when cross-correlating the associated signal and idler images. We thus need to consider in the computation of the cross-correlation coefficient a contribution related to accidental coincidences of independent events, but also a fluctuation of the twin and accidental coincidences due to the random nature of the events. The reconstruction of the time signal can be performed properly in a single operation only if we can distinguish at least two levels in the signal (case of a binary signal). For a Gaussian distribution, this distinction is feasible in 99.3% of cases if the signal to noise ratio SNR_n associated to the step n verifies

$$SNR_n = \frac{C_n}{\sigma_n} \geqslant 2.45\, L\, T_n \tag{1}$$

where σ_n is the overall standard deviation of the number of coincidences, $L = 2$ is the number of levels in the signal, T_n is the binary transmission ($T_n = 0$ or 1) induced by the variable attenuation for the step n of the time signal, and C_n is the mean total number of twin coincidences between the sum picture S and the idler image I_n. The value $2.45 \times \sigma$ represents the abscissa at which the cumulative density function of a Gaussian distribution takes a value 99.3%.

The average number of accidental coincidences is shifted to zero by removing in each picture the deterministic shape of the SPDC beams. This step ensures the statistical independence of two non-twin images. Two effective methods can be applied here. The first one consists of assimilating the shape of the SPDC beam as a Gaussian, since the intensity of the SPDC beams is proportional to the intensity of the pump beam. Each signal and idler picture is fitted by a Gaussian profile that is then removed from the image. This method is efficient if the experiment is limited to the retrieval of a unique time signal and not repeated [15]. However, if the shape of the beams is not perfectly Gaussian, this method could leave some residual deterministic correlations. The second method consists of recording a large number of images to determine the average deterministic shape of the signal and idler beams as a calibration of the system. The average shape is then removed from each picture before performing the cross-correlation [14]. If feasible, this last method is slightly more efficient and much more rapid. It will be used in the following.

C_n can be determined from our experimental parameters, after this subtraction, as [13]

$$C_n \simeq T_n D(\eta m_i - m_i^2) \tag{2}$$

where m_i is the mean number of photons (events) per pixel of the idler images. The approximation is valid if the incident photon flux per time step m_i/η is much smaller than one, which allows the probability of two photons incident on the same pixel to be neglected.

σ_n takes into account the fluctuations of both twin and accidental coincidences:

$$\sigma_n = (V_{c,n} + V_{a,n})^{1/2} \tag{3}$$

where $V_{c,n}$ and $V_{a,n}$ are respectively the variances of the total number of twin and accidental coincidences between S and I_n at the location of the peak. Because of the Poissonian distribution of the SPDC pattern, we have directly $V_{c,n} = C_n$. Since $V_{a,n}$ is not related to the number of twin coincidences between the signal-integrated image S and one of the idler reference images I_n, it does not depend on the step n, and consequently $V_{a,n} = V_a$. Its value can be assessed as follows, in a similar manner as in [13]. We want to assess the fluctuations of $\widehat{\mathrm{cov}}(N_s, N_{i_k})$, the estimator of the covariance between one pixel s of the signal picture S and the same pixel $i_k = s$ of the idler picture I_k, for independent events (no twin coincidences). N_s and N_{i_k} are the intensities of the s and i_k pixels that are in our case either 1 for one photon or 0 for no photons. $\widehat{\mathrm{cov}}(N_s, N_{i_k})$ is given for each couple $s = i_k$ of the area D by

$$\begin{aligned}\widehat{\mathrm{cov}}(N_s, N_{i_k}) &= \frac{1}{D}\sum_{s=i_k=1}^{D}(N_s - \overline{N_s})(N_{i_k} - \overline{N_{i_k}}) \\ &= \overline{N_s N_{i_k}} - \overline{N_s}\,\overline{N_{i_k}}.\end{aligned} \tag{4}$$

Because of the independence of the events, $\langle\widehat{\mathrm{cov}}(N_s, N_{i_k})\rangle = 0$, where $\langle\rangle$ stands for the true mean (mathematical expectation). In the second term of equation (4), the variance of $\overline{N_s}\,\overline{N_{i_k}}$ is negligible with respect to the variance of $\overline{N_s N_{i_k}}$. The only possible values of N are 0 and 1. Hence, we have

$$\begin{aligned}\mathrm{var}(\overline{N_s N_{i_k}}) &= \frac{1}{D}(\langle(N_s N_{i_k})^2\rangle - \langle N_s N_{i_k}\rangle^2) \\ &= \frac{1}{D}m_s m_i - (m_s m_i)^2 \simeq \frac{1}{D}m_s m_i\end{aligned} \tag{5}$$

where m_s and m_i are the true means of the signal and idler images, respectively. In the last approximative equality, we assume that m_s and m_i are both $\ll 1$.

The total number of coincidences is given also by equation (4), but without the division by the number of pixels. Hence we have, if there is no binning,

$$V_a = \mathrm{var}\left(\sum_{s=i_k=1}^{D} N_s N_{i_k}\right) = D\, m_s m_i. \tag{6}$$

The last step consists of calculating the variance V_a of the total number of coincidences between two areas obtained by summing B adjacent pixel values of the correlation image:

$$V_a = \mathrm{var}\left(\sum_{b=1}^{B}\sum_{s=i_k=1}^{D} N_s N_{i_k}\right) = D\, B\, m_s m_i. \tag{7}$$

The signal to noise ratio hence becomes

$$SNR_n = \frac{T_n D(\eta m_i - m_i^2)}{(T_n D\eta m_i + DB\, m_s m_i)^{1/2}}. \tag{8}$$

Because of the binning B, the second term of the denominator, due to accidental coincidences, is much greater than the first term due to the fluctuations of the number of twin coincidences. By neglecting this first term and the second term of the numerator, and by assuming a binary signal with M bits at one, we obtain an approximation of SNR_n as

$$SNR_n \simeq T_n \eta\left(\frac{D}{B\,M}\right)^{1/2}. \tag{9}$$

The approximation of equation (9), though not very precise (the second term of the numerator is not completely negligible), gives us a practical clue. We have to find an optimal compromise for the binning: increasing B allows the surface of the cross-correlation peak to be entirely covered, resulting in an increase of η but at the expense of a decreasing of the number of resolution cells D/B . Experimentally, the lowest error rate has been attained for a binning of five pixels on the y axis and 16 pixels on the x axis. This reduced binning unfortunately brings us to ignore the fourth of the coincidences that are situated on pixels outside the position of the binned peak. The equivalent quantum efficiency thus becomes $\eta = 23\%$.

By taking into account these values, we have chosen to perform the reconstruction of a time signal of two levels (binary) and eight steps that should result in a SNR around 6.

4. Experimental application

Although the purpose of the experiment is to benefit of a safe reconstruction on a single operation, the process is repeated 990 times. This allows the estimation of the average experimental SNR on the reconstructed steps. The ghost signal reconstructed here is made of four bits at '1' and four bits at '0'. The reconstruction shown in figure 3 displays the average cross-correlation coefficient of each step of the time signal, given as a number of coincidences. Let us recall that the average images have been subtracted, meaning that the mean numbers of accidental coincidences have been set to 0 even if these accidental coincidences are the main source of noise, as shown previously. The error bars represent the experimental standard deviation of the computed numbers of coincidences associated with each step.

The SNR of the steps '1' is here equal to 4.9, while a direct application of equation (8) gives a SNR of 6.3. The most important factors that explain this difference between are:

- The Gaussian shape of the beams results in an effective number of pixels which is smaller than the number D of the physical pixels.
- In the low-light-level parts of the image, the detector noises are more important than those taken into account by the effective quantum efficiency.

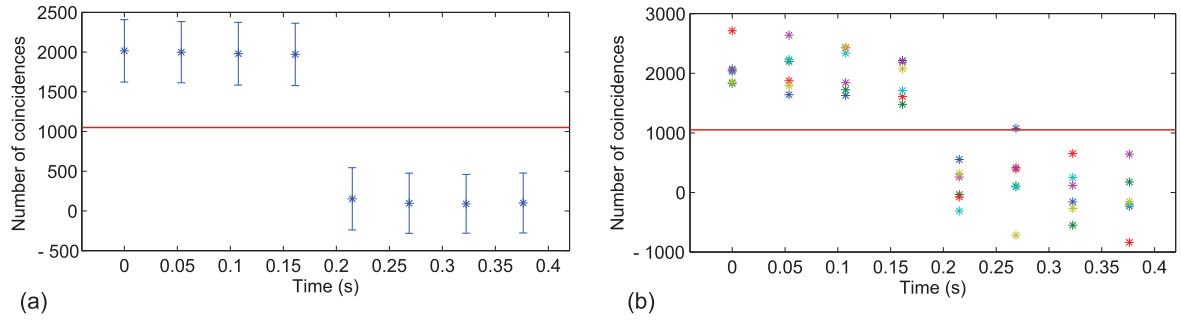

Figure 3. (a) Average on 990 reconstructions. The blue dots are the average numbers of coincidences as given in equation (2), and the error bars are their standard deviation. (b) Superposition of five reconstructions. The full red line represents the threshold situated at the half average number of coincidences for the '1' steps.

– The fluctuations of the pixels in the correlation image are not completely independent, probably because of some smearing. Experimentally, for $B = 1$, the standard deviation of the correlation image has a value outside the twin peak equal to 37.3—in rather good agreement with its theoretical value $D(m_s m_i)^{1/2} = 35.8$. On the other hand, its value of 373 for $B = 80$ is greater than the expected 320.

The error rate of 0.7% is in full agreement with the experimentally measured SNR. It has been obtained by a simple method of thresholding, where a threshold (red full line in figure 3) is placed at the middle between the mean 1 level and the 0 one.

5. Conclusion

We showed in this experiment of temporal ghost imaging that it is possible to reconstruct single sequences of time signals using quantum correlated photons of SPDC. The number of coherence cells contained in the images determines the available whole length and the error rate in the reconstruction process. The relatively low value of this number, around 3000 here, can be increased in two ways:

– A thinner crystal allows the size of a coherence cell in the image plane to decrease by increasing the phase-matching range in the Fourier plane.
– A wider crystal allows the number of coherence cells in a transverse section to increase.

However, the conservation of the SPDC gain would require a more powerful pump beam, as the surface illuminated is larger and the interaction time between the pump pulses and the crystal is smaller. Likewise, more efficient detectors and a reduction of the parasitic fluorescence could result in an increase of the equivalent quantum efficiency. The phase-matching constraints explain that performances remain below that obtained by classical means [7, 8]. Nevertheless, this experiment shows that temporal ghost imaging can be performed by using either twin photons or classical correlations, just as for spatial ghost imaging.

Funding

This work was supported by the Labex ACTION program (ANR-11-LABX-0001-01).

References

[1] Pittman T B, Shih Y H, Strekalov D V and Sergienko A V 1995 Optical imaging by means of two-photon quantum entanglement *Phys. Rev.* A **52** R3429
[2] Morris P A, Aspden R S, Bell J E C, Boyd R W and Padgett M J 2015 Imaging with a small number of photons *Nat Commun.* **6** 5913
[3] Bennink R S, Bentley S J and Boyd R W 2002 Two-photon coincidence imaging with a classical source *Phys. Rev. Lett.* **89** 113601
[4] Ferri F, Magatti D, Gatti A, Bache M, Brambilla E and Lugiato L A 2005 High-resolution ghost image and ghost diffraction experiments with thermal light *Phys. Rev. Lett.* **94** 183602
[5] Gatti A, Brambilla E, Bache M and Lugiato L A 2004 Correlated imaging, quantum and classical *Phys. Rev.* A **70** 013802
[6] Ryczkowski P, Barbier M, Friberg A T, Dudley J M and Genty G 2016 Ghost imaging in the time domain *Nat Photonics* **10** 167
[7] Devaux F, Moreau P-A, Denis S and Lantz E 2016 Computational temporal ghost imaging *Optica* **3** 698
[8] Devaux F, Huy K P, Denis S, Lantz E and Moreau P-A 2017 Temporal ghost imaging with pseudo-thermal speckle light *J. Opt.* **19** 024001
[9] Shapiro J H 2008 Computational ghost imaging *Phys. Rev.* A **78** 061802
[10] Bromberg Y, Katz O and Silberberg Y 2009 Ghost imaging with a single detector *Phys. Rev.* A **79** 053840
[11] Cho K and Noh J 2012 Temporal ghost imaging of a time object, dispersion cancelation, and nonlocal time lens with bi-photon state *Opt. Commun.* **285** 1275
[12] Lantz E, Blanchet J-L, Furfaro L and Devaux F 2008 Multi-imaging and Bayesian estimation for photon counting with EMCCDs *Mon. Not. R. Astron. Soc.* **386** 2262
[13] Lantz E, Moreau P-A and Devaux F 2014 Optimizing the signal-to-noise ratio in the measurement of photon pairs with detector arrays *Phys. Rev.* A **90** 063811
[14] Moreau P-A, Devaux F and Lantz E 2014 Einstein-Podolsky-Rosen paradox in twin images *Phys. Rev. Lett.* **113** 160401
[15] Lantz E, Denis S, Moreau P-A and Devaux F 2015 Einstein-Podolsky-Rosen paradox in single pairs of images *Opt. Express* **23** 26472